Statistical thermodynamics of adsorbates with nonsymmetrical lateral interactions

F. Romá and A. J. Ramirez-Pastor*

Departamento de Física, Universidad Nacional de San Luis, CONICET, Chacabuco 917, 5700 San Luis, Argentina

(Received 16 December 2002; revised manuscript received 12 January 2004; published 31 March 2004)

The exact adsorption thermodynamics of particles with nonsymmetrical ad-ad interactions on a one-dimensional space is presented. The asymmetry is introduced by considering the lateral interactions depending on the orientation of the adsorbed molecules. The adsorption process is monitored by following the adsorption isotherm, the thermodynamic factor, the differential heat of adsorption, and the configurational entropy of the adlayer. A rich variety of different behaviors is found with respect to the standard lattice gas of interacting monomers. The resulting thermodynamic description may also be applicable to adsorption and transport of nonspherical molecules in low-dimensional systems such as carbon nanotubes.

DOI: 10.1103/PhysRevE.69.036124 PACS number(s): 05.50.+q, 05.10.Ln, 02.10.Yn, 68.35.Md

I. INTRODUCTION

In the scientific literature of the last years, it is possible to find many theoretical works concerning physicochemical of adsorption [1–6]. Most of these studies are based on generalizations of the standard lattice-gas theory [7], including ad-ad interactions, surface heterogeneity, multilayer adsorption, etc. [4,6,8–12]. However, in all cases, the models preserve a fundamental statistical property, the well-known symmetry particle vacancy.

Recent molecular simulations [13–16] and experimental developments [17,18] about the adsorption of different gases in low-dimensional systems have shown clear signals of nonequivalence between particles and vacancies. In fact, adsorption isotherms for methane, ethane, and others adsorbed on $AlPO_4-5$ and $SAPO-5$ are clearly unsymmetrical around half coverage. These phenomena are also visible in the isosteric heat of adsorption.

The main routes to break the symmetry particle vacancy are the following: (1) to consider three-particle interactions; (2) to introduce some sort of local correlation, such as particles that occupy several k contiguous lattice sites (k mers); (3) to consider pairwise lateral interactions depending on the orientation of the adsorbate.

Point (1) is widely discussed in Ref. [19]. Works including multisite occupancy [20–24] (or adsorption of k mers) present two additional difficulties, which differentiate the k-mers statistics from the usual single-particle statistics. They are the following: (i) the occupation of a given lattice site ensures that at least one of its nearest-neighbor sites is also occupied, and (ii) an isolated vacancy cannot serve to determine whether or not that site can ever become occupied. For these reasons, it has been difficult to formulate, in an analytical way, the statistics (and kinetics) of occupation for correlated particles.

In the present work, nonequivalence between particle and vacancy is included as in point (3), preserving the simplicity of the single-particle statistics. For this purpose, a nonsymmetrical lattice gas of monomers is considered. The system is exactly solved by using the transfer matrix method (TMM) in grand canonical ensemble. This paper has several objectives: (i) To obtain the exact solution for a generalized lattice gas of nonsymmetrical interacting particles adsorbed on a one-dimensional substrate; (ii) to identify and characterize the most prominent features of this particular process; (iii) to develop a simpler and manageable model, capable to reproduce experimental findings where the adsorption involves nonsymmetrical lateral interactions and low-dimensional substrates; (iv) to stimulate the development of more complex models including nonsymmetrical interactions and nonspherical adsorbates.

The organization of the paper is as follows. In Sec. II we present the model and a brief description of how the partition function and other quantities can be calculated exactly from the transfer matrix method. The predictions of the theoretical calculations are presented and discussed in Sec. III. Finally, the conclusions are drawn in Sec. IV.

II. MODEL AND TRANSFER MATRIX METHOD

The transfer matrix method has widely been used in surface science. In fact, different surface phenomena (such as multisite-occupancy adsorption [21,25], thermal desorption [26,27], surface diffusion, adsorption isotherms [28,29], etc.) have been investigated by using TMM. In the present work, the technique has been extended to nonsymmetrical interacting particles.

Let us assume a one-dimensional homogeneous lattice of M sites with lattice constant a ($M\rightarrow\infty$) where periodic boundary conditions apply. Under this condition all lattice sites are equivalent hence border effects will not enter our derivation.

N monomers are adsorbed on the lattice in such a way that a monomer occupies one lattice site and double-site occupancy is not allowed as to represent properties in the monolayer regime. Each monomer (circle in Fig. 1) is a nonsymmetrical particle consisting of two different groups (each denoted by black or white semicircles in Fig. 1). In this way, we distinguish two kinds of monomers: (1) [(2)] black-white [white-black] monomers, which are absorbed on the lattice with the black [white] side at left and the white [black] side at right. For a given N, there exists N_1 (N_2) black-white (white-black) particles adsorbed, being $N=N_1+N_2$.

*Author to whom correspondence should be addressed.

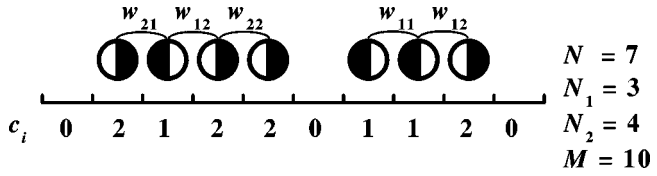

FIG. 1. Schematic representation of the different energies involved in the adsorption process.

In order to describe the system of N asymmetric monomers adsorbed on M sites at a given temperature T, let us introduce the occupation variable c_i which can take the following values: $c_i=0$ if the corresponding site is empty, $c_i=1$ if the site is occupied by a black-white monomer, and $c_i=2$ if the site is occupied by a white-black monomer. The energies involved in the adsorption process are five (see Fig. 1): (1) U, interaction energy between a monomer (black-white or white-black monomer) and a lattice site; (2) w_{11}, nearest-neighbor interaction energy between two black-white monomers; (3) w_{22}, nearest-neighbor interaction energy between two white-black monomers; (4) w_{12}, nearest-neighbor interaction energy between a black-white monomer at left and a white-black monomer at right; (5) w_{21}, nearest-neighbor interaction energy between a white-black monomer at left and a black-white monomer at right.

Under these considerations, the Hamiltonian of the system is given by

$$H=\sum_{i=1}^{M}\left[w_{11}\delta_{c_i,1}\delta_{c_{i+1},1}+w_{22}\delta_{c_i,2}\delta_{c_{i+1},2}+w_{12}\delta_{c_i,1}\delta_{c_{i+1},2}+w_{21}\delta_{c_i,2}\delta_{c_{i+1},1}\right]+(U-\mu)\sum_{i=1}^{M}(\delta_{c_i,1}+\delta_{c_i,2}), \tag{1}$$

where the symbol δ represents the Kronecker delta function and w_{ij} is assumed to be repulsive (positive) or attractive (negative). Finally, since the lattice is assumed homogeneous, U is set equal to zero for simplicity, without any loss of generality.

The grand partition function Ξ is

$$\Xi(\mu,T)=\sum_{c_1}\sum_{c_2}\cdots\sum_{c_M}\exp(-\beta H), \tag{2}$$

where $\beta=1/k_BT$ and k_B is the Boltzmann constant.

By defining the transfer matrix Q as

$$Q_{\alpha,\gamma}=\langle\alpha|Q|\gamma\rangle=\exp\{-\beta[w_{11}\delta_{\alpha,1}\delta_{\gamma,1}+w_{22}\delta_{\alpha,2}\delta_{\gamma,2}+w_{12}\delta_{\alpha,1}\delta_{\gamma,2}+w_{21}\delta_{\alpha,2}\delta_{\gamma,1}]\}\times\exp[\beta\mu(\delta_{\alpha,1}+\delta_{\alpha,2})]\quad(\alpha,\gamma=0,1,2). \tag{3}$$

In addition,

$$c_i=0\Leftrightarrow|0\rangle\Leftrightarrow\begin{pmatrix}1\\0\\0\end{pmatrix}, \tag{4}$$

$$c_i=1\Leftrightarrow|1\rangle\Leftrightarrow\begin{pmatrix}0\\1\\0\end{pmatrix}, \tag{5}$$

$$c_i=2\Leftrightarrow|2\rangle\Leftrightarrow\begin{pmatrix}0\\0\\1\end{pmatrix}. \tag{6}$$

Then, the matrix Q can be written as

$$Q=\begin{pmatrix}1&1&1\\ \lambda&\lambda x_{11}&\lambda x_{12}\\ \lambda&\lambda x_{21}&\lambda x_{22}\end{pmatrix}, \tag{7}$$

where $\lambda=\exp(\beta\mu)$ is the fugacity and $x_{ij}=\exp(-\beta w_{ij})$ is the absolute activity associated with the interaction energy $w_{ij}=(w_{11},w_{12},w_{21},\text{ or }w_{22})$.

Now, we can write the grand partition function by using the elements of Q:

$$\Xi(M,\lambda,T)=\sum_{c_1}\sum_{c_2}\cdots\sum_{c_M}\langle c_1|Q|c_2\rangle\times\langle c_2|Q|c_3\rangle\cdots\langle c_M|Q|c_1\rangle. \tag{8}$$

Due to the closure relation $\Sigma_{ci}|c_i\rangle\langle c_i|=\mathbf{1}$, the last expression of Ξ can be simplified as

$$\Xi(M,\lambda,T)=\sum_{c_1}\langle c_1|Q^M|c_1\rangle=\mathrm{Tr}(Q^M)=q_1^M+q_2^M+q_3^M, \tag{9}$$

where $\{q_1,q_2,q_3\}$ is the set of eigenvalues of the (3×3) matrix Q. In addition, in the thermodynamical limit ($M\to\infty$),

$$\lim_{M\to\infty}\left[\frac{\ln\Xi(M,\lambda,T)}{M}\right]=\ln q_1, \tag{10}$$

where q_1 is the largest eigenvalue of Q.[1]

The grand partition function was obtained through a standard software to compute the eigenvalues of a matrix.

The main thermodynamic functions can be obtained from the grand partition function [7]:

$$\overline{N}=\lambda\left[\frac{\partial\ln\Xi(M,\lambda,T)}{\partial\lambda}\right]_{M,T}, \tag{11}$$

[1] $\ln(q_1^M+q_2^M+q_3^M)=\ln[1+(q_2/q_1)^M+(q_3/q_1)^M]+M\ln q_1$. Then, if q_1 is the largest eigenvalue of Q and $M\to\infty$, $\ln(q_1^M+q_2^M+q_3^M)/M=\ln q_1$.

$$\frac{S}{k_B} = T\left(\frac{\partial \ln \Xi(M,\lambda,T)}{\partial T}\right)_{M,\lambda} + \ln \Xi(M,\lambda,T), \quad (12)$$

$$E = -\left[\frac{\partial \ln \Xi(M,\lambda,T)}{\partial \beta}\right]_{M,\lambda}, \quad (13)$$

where $\overline{N}$, S, and E designate the mean number of particles in the adlayer, the entropy, and the total energy, respectively.

III. RESULTS

We focus on the case of repulsive lateral interactions among adsorbed particles ($w_{ij}>0$) since, as we shall see, different structures appear in the adsorbed phase.

In order to rationalize our analysis, seven different cases have been considered, according to the lateral interaction energies involved in the adsorption process:

Case I. $w_{11}=w_{12}=w_{21}=w_{22}=w>0$.

Case II. $w_{11}=w_{12}=w_{22}=w>0$ and $w_{21}=0$ (or $w_{11}=w_{21}=w_{22}=w>0$ and $w_{12}=0$).

Case III. $w_{11}=w>0$ and $w_{12}=w_{21}=w_{22}=0$ (or $w_{22}=w>0$ and $w_{12}=w_{21}=w_{11}=0$).

Case IV. $w_{12}=w>0$ and $w_{11}=w_{21}=w_{22}=0$ (or $w_{21}=w>0$ and $w_{11}=w_{12}=w_{22}=0$).

Case V. $w_{11}=w_{22}>0$ and $w_{12}=w_{21}=0$.

Case VI. $w_{11}=w_{12}=w>0$ and $w_{21}=w_{22}=0$ (or $w_{22}=w_{21}=w>0$ and $w_{12}=w_{11}=0$).

Case VII. $w_{11}=w_{12}=w_{21}=w>0$ and $w_{22}=0$ (or $w_{22}=w_{12}=w_{21}=w>0$ and $w_{11}=0$).

From the theoretical point of view, cases I–VII can be separated in three groups: (i) Cases I, II, IV, and V correspond to identical nonsymmetrical particles adsorbed on homogeneous surfaces (where $w_{11}=w_{22}$); (ii) cases III and VII represent adsorption of two different symmetrical particles on homogeneous surfaces (where $w_{11}\neq w_{22}$ and $w_{12}=w_{21}$), and (iii) case VI corresponds to two different nonsymmetrical particles adsorbed on homogeneous surfaces (where $w_{11}\neq w_{22}$ and $w_{12}\neq w_{21}$).

On the other hand, the experimental realizations of carbon nanotubes and synthetic zeolites as $AlPO_4-5$ and SAPO -5 have greatly stimulated the study of vapors and liquids confined in low-dimensional adsorption potentials. These materials literally provide the route to the realization of one-dimensional (1D) adsorbents. Among the studied systems, the adsorption of CH_4 in $AlPO_4-5$ has been widely treated in the literature [13–18]. These papers predict a complex behavior. At low temperatures, Radhakrishnan *et al.* [15] have reported, by using molecular simulations, a phase transition occurring between two different density states, one corresponding to a low density (''gas'') and the other to a higher density (''liquid'') phase. The authors propose that this transition is induced by the interactions with the molecules that are in neighboring channels. A different type of transition was found by Boutin *et al.* [13] and Lachet *et al.* [14] at intermediate temperatures (much higher temperature than the phase transition considered by Radhakrishnan *et al.*). The molecular simulations of Refs. [13,14] show stepped isotherms. The step was only observed using a model that includes both two-body and three-body lateral interactions, whereas a model with only two-body interactions did not show such a step. Recently, this transition has been confirmed by experimental results by Martin *et al.* [17,18]. The step was attributed to local rearrangement of the adsorbed phase: first the fluid phase gives rise to a quasi-1D structure with four molecules per unit cell, which looks like CH_4 dimers chain. At higher coverage, a second structure with six molecules per unit cell grows up to form a chain of methane trimers [17,18].

In this context, cases I, II, and intermediate cases (obtained by mixing cases I and II) are far more interesting, since structural rearrangement which takes place in the adsorbate and double-stepped isotherms can be obtained. The application of these cases as a possible model for understanding the structural transition occurring in $CH_4/AlPO_4-5$ will be extensively discussed at the end of this section.

To study the temperature dependence, we fix $w=1$ and vary k_BT. The results for cases I–VII are presented in the following.

For case I, and due to the symmetry of the interactions, it is possible to obtain exact closed expressions for the thermodynamical functions. For this purpose, we can think of a mapping from the exact solution of the well-known lattice gas of symmetrical monomers [7] to the corresponding system of nonsymmetrical particles. The only difference is associated with considering the two possible orientations of the nonsymmetrical molecules. Accordingly, the partition functions[2] in both systems are related through

$$Q(M,N,T) = 2^N Q^s(M,N,T), \quad (14)$$

where Q (Q^s) represents the partition function corresponding to nonsymmetrical (symmetrical) monomers.

In the canonical ensemble the Helmholtz free energy $F(M,N,T)$ relates to $Q(M,N,T)$ through

$$\beta F(M,N,T) = -\ln Q(M,N,T). \quad (15)$$

The remaining thermodynamic functions can be obtained from the general differential form [7]

$$dF = -SdT - \Pi dM + \mu dN, \quad (16)$$

where S, Π, and μ designate the entropy, spreading pressure, and chemical potential, respectively, which, by definition, are

$$S = -\left(\frac{\partial F}{\partial T}\right)_{M,N}, \quad \Pi = -\left(\frac{\partial F}{\partial M}\right)_{T,N}, \quad \mu = \left(\frac{\partial F}{\partial N}\right)_{T,M}. \quad (17)$$

For symmetrical monomers, the partition function Q^s can be obtained exactly by using the cumulant variation method [30,31]. Thus,

[2] In this point, we work in the canonical ensemble for simplicity. Note the simple relationship between Q and Q^s in Eq. (14).

$$-\ln Q^s(\theta,T)=\beta wy-\theta\ln\theta-(1-\theta)\ln(1-\theta)+y\ln y$$
$$+2(\theta-y)\ln(\theta-y)$$
$$+(1-2\theta-y)\ln(1-2\theta-y), \quad (18)$$

where Q^s has been written in terms of the surface coverage $\theta=N/M$. In addition,

$$y=\theta-\left(\frac{A}{2}\right)+\left[\frac{A^2}{4}-\theta(1-\theta)A\right]^{1/2}, \quad (19)$$

where $A=[1-\exp(-\beta w)]^{-1}$ and w is the lateral interaction between two nearest-neighbor symmetrical monomers. Finally, the chemical potential and the entropy per site, s, for nonsymmetrical monomers are straightforward from Eqs. (14)–(19),

$$\beta\mu=\beta w+\ln[b-1+2\theta]-\ln[b+1-2\theta]-\ln 2 \quad (20)$$

and

$$s/k_B=\theta\ln\theta+(1-\theta)\ln(1-\theta)-2\alpha\ln\alpha-(\theta-\alpha)\ln(\theta-\alpha)$$
$$-(1-\theta-\alpha)\ln(1-\theta-\alpha)+\theta\ln 2, \quad (21)$$

where α is given by

$$\alpha=\frac{2\theta(1-\theta)}{(1+b)} \quad \text{and} \quad b=\left[1-\frac{4}{A}(\theta-\theta^2)\right]^{1/2}. \quad (22)$$

In Fig. 2, we show the adsorption isotherm (a) and the configurational entropy per site of the adsorbate (in k_B units) (b) for case I. The symbols correspond to results of TMM and the solid lines to modified symmetrical monomer model (MSMM). The agreement between the curves validates the calculations obtained by using TMM.

For high temperatures, the isotherms tend to the Langmuir case. As T decreases, the isotherms develop a neat plateau at $\theta=1/2$. Particles avoiding configurations with nearest-neighbor repulsive order in a structure of alternating adatoms separated by an empty site at $\theta=1/2$. The width of the step is directly proportional to the energy per particle necessary to alter such an ordered structure.

With respect to the entropy , the overall behavior can be summarized as follows. For high temperatures and low coverage, $s(\theta)/k_B$ is an increasing function of θ, reaches a maximum at $\theta\approx 0.65$, and then decreases monotonically to $\ln 2$ for $\theta=1$. This value at full coverage is related to the two possible states, $c_i=1$ or 2, for each adsorption site.

As the temperature is diminished, the entropy decreases for all coverage and develops a local minimum at $\theta=1/2$. The origin of this minimum is the structure discussed above for the adsorption isotherm. In the ground state and $\theta=1/2$, each occupied site has two possible states and $s(\theta=1/2,T=0)/k_B=0.5\ln 2$.

In order to compare with the case of symmetrical particles, in Fig. 2(b) we included the curves for the entropy of symmetrical monomers in the limit cases: $T=\infty$ (dashed line) and $T=0$ (dotted line). In both cases, the curves present symmetry with respect to $\theta=1/2$. In addition, in the ground state, $s(\theta=1/2,T=0)/k_B=0$.

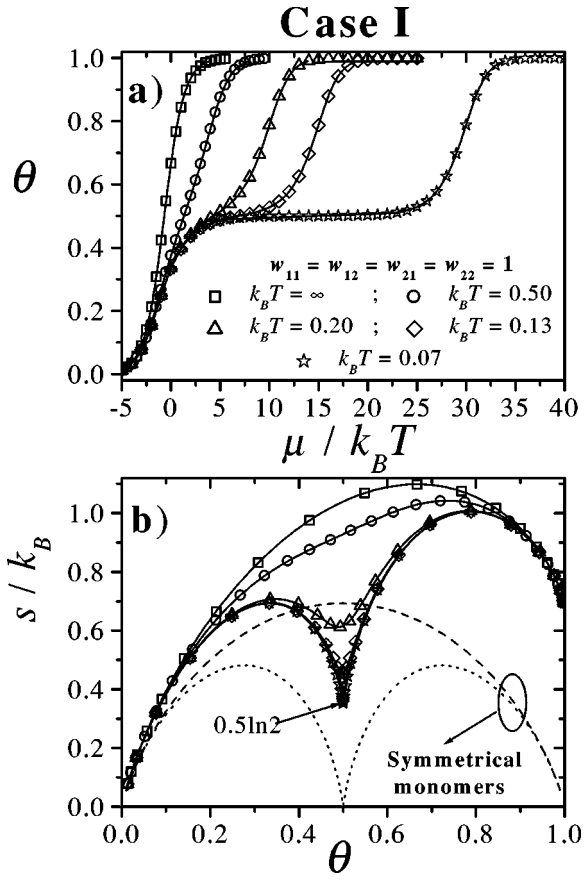

FIG. 2. Adsorption isotherm (a) and configurational entropy per site vs coverage (b) for case I. The curves were obtained for $w=1$ and different values of k_BT (as shown in the figure). Symbols (solid lines) correspond to results obtained by using TMM (MSMM). In (b), dashed and dotted lines represent the entropy of symmetrical monomers for $T=\infty$ and $T=0$, respectively.

The results for case II are shown in Fig. 3. An interesting behavior for the adsorption isotherm (a) and the configurational entropy per site (b) occurs as the temperature is diminished. In this condition, the isotherm (entropy) develops a plateau (minimum) in $\theta=\theta_m$, which depends on the temperature.[3] These singularities reflect clearly two adsorption regimes: (i) in the first regime ($0\leqslant\theta<\theta_m$), the particles adsorb on the lattice avoiding 11, 12, and 22 lateral interactions; and (ii) in the second regime ($\theta_m<\theta<1$), the filling is completed.

The position of the minimum in the entropy, θ_m, is a function of T. In Fig. 4(a), we show how $\theta_m(T)$ goes to 2/3 in the ground state. On the other hand, the value of the entropy in θ_m tends to zero as the temperature is decreased. In the ground state and $\theta=2/3$, the structure of the adlayer is characterized by an alternating repetition of the sequence

[3]On the contrary, this plateau (minimum) remains fixed at half coverage for case I [see Fig. 2(b)].

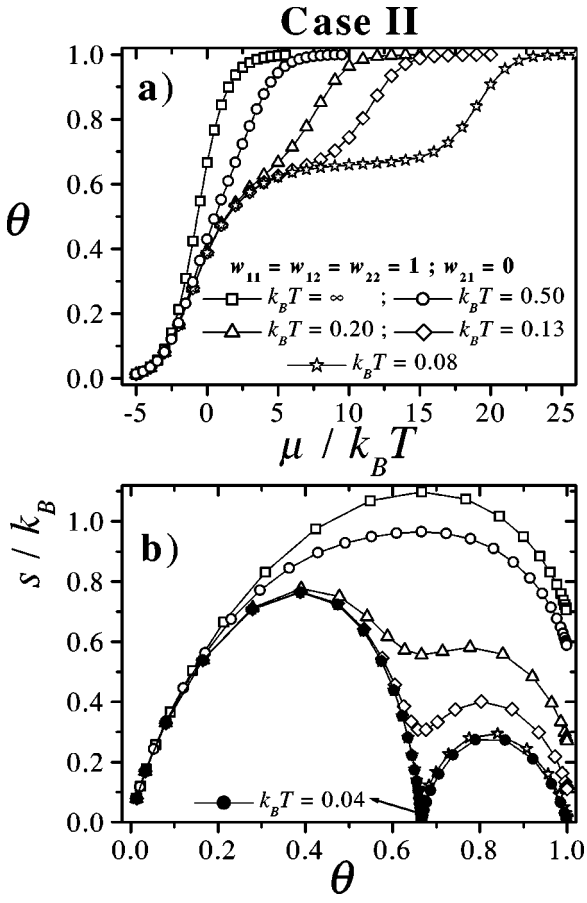

FIG. 3. Adsorption isotherm (a) and configurational entropy per site vs coverage (b) for case II. The curves were obtained for $w=1$ and different values of k_BT (as shown in the figure).

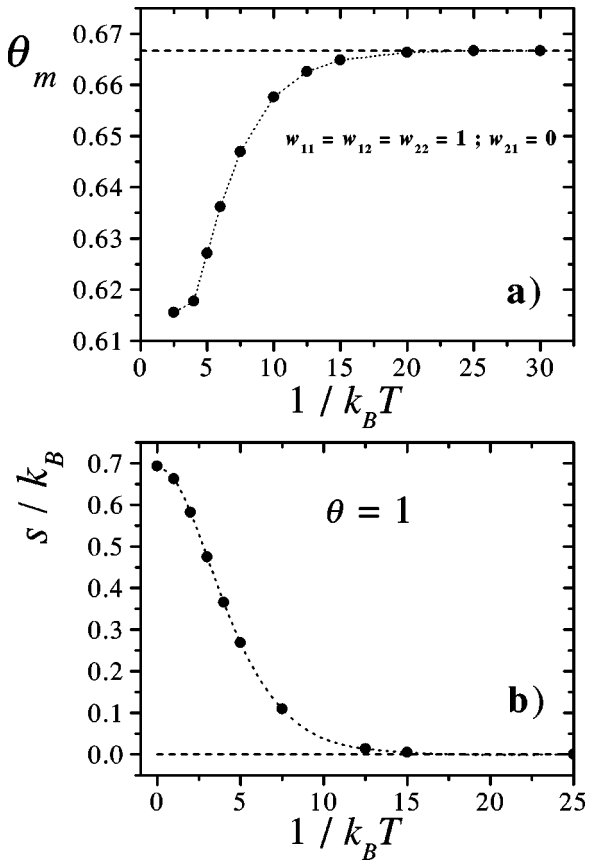

FIG. 4. (a) Temperature dependence of the position of the minimum in the entropy, $\theta_m(T)$, for case II. (b) Idem to (a) for the configurational entropy per site at full coverage, $s(\theta=1,T)/k_B$.

(210), corresponding to $c_i=2, c_{i+1}=1$, and $c_{i+2}=0$. Since this structure can be shifted in one or two sites, the degeneration of this state is three and the entropy per site is zero in the thermodynamical limit.

Another interesting characteristic of the curves in Fig. 3(b) is related to the value of the entropy for $\theta=1$, which depends on T. In fact, as is shown in Fig. 4(b), $s(\theta=1,T)/k_B$ decreases as the temperature is diminished. In the limit case of $T=0$, a structure of alternating different particles (12121212 . . . .) is formed at full coverage. The degeneration of this structure is two and the entropy per site is zero as $M\to\infty$ $[s(\theta=1,0)/k_B=0]$.

Figure 5 shows the adsorption isotherm (a) and the configurational entropy per site versus coverage (b) for case III. As the temperature is varied, the adsorption isotherms do not change appreciably. However, the configurational entropy is more sensitive to the variation of the temperature. The overall effect of the temperature is a decrease of s/k_B for all coverage as T decreases. In particular, the value of the entropy at full coverage, $s(\theta=1)/k_B$, varies between $\ln 2$ (for $T=\infty$) and 0.4812 (for $T=0$). The complete temperature dependence of $s(\theta=1)/k_B$ is shown in the inset of the Fig. 5(b).

The value $s(\theta=1,T=0)/k_B=0.4812$ can be explained as follows: let us consider a lattice of M sites at full coverage; then, the number of different configurations (degeneracy) of the ground state, g_M, can be written as

$$g_M = AB^M + C, \tag{23}$$

where A, $B>1$, and C are constants. Equation (23) represents a general expression for g_M, providing $s=k_B\ln g_M>0$ in the thermodynamical limit. Then,

$$\frac{s(\theta=1,T=0)}{k_B} = \lim_{M\to\infty}\frac{\ln g_M}{M}$$

$$= \ln B + \lim_{M\to\infty}\frac{1}{M}\ln\left(A+\frac{C}{B^M}\right) = \ln B. \tag{24}$$

In addition, in the particular case of $w_{11}=w>0$ and $w_{12}=w_{21}=w_{22}=0$, it is easy to demonstrate (see the Appendix) that

$$g_M = g_{M-1} + g_{M-2}. \tag{25}$$

From Eqs. (23) and (25), the value of B can be calculated as

$$AB^M + C = AB^{M-1} + C + AB^{M-2} + C$$

$$B^2 = B + 1 + \frac{C}{AB^{M-2}}. \tag{26}$$

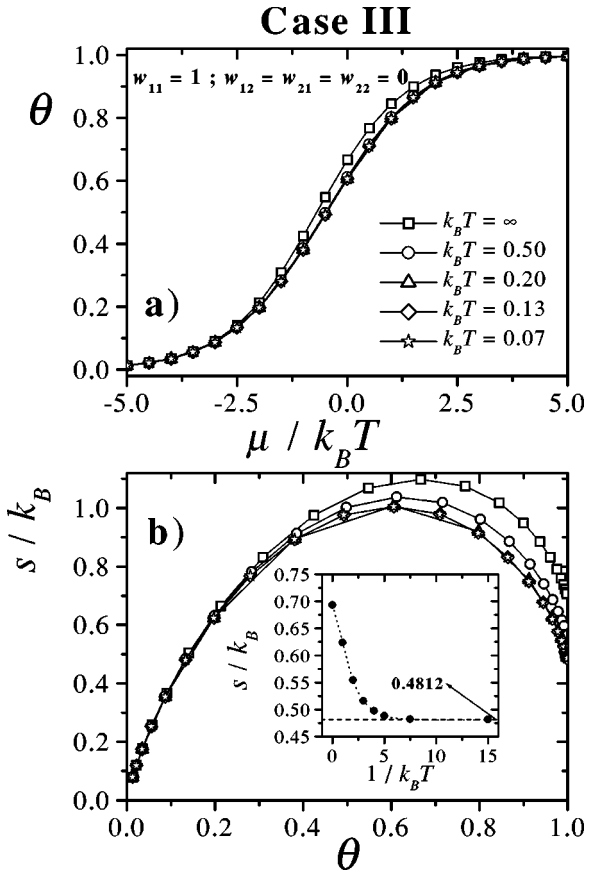

FIG. 5. As Fig. 3 for case III. In the inset, we represent the temperature dependence of the configurational entropy per site at full coverage.

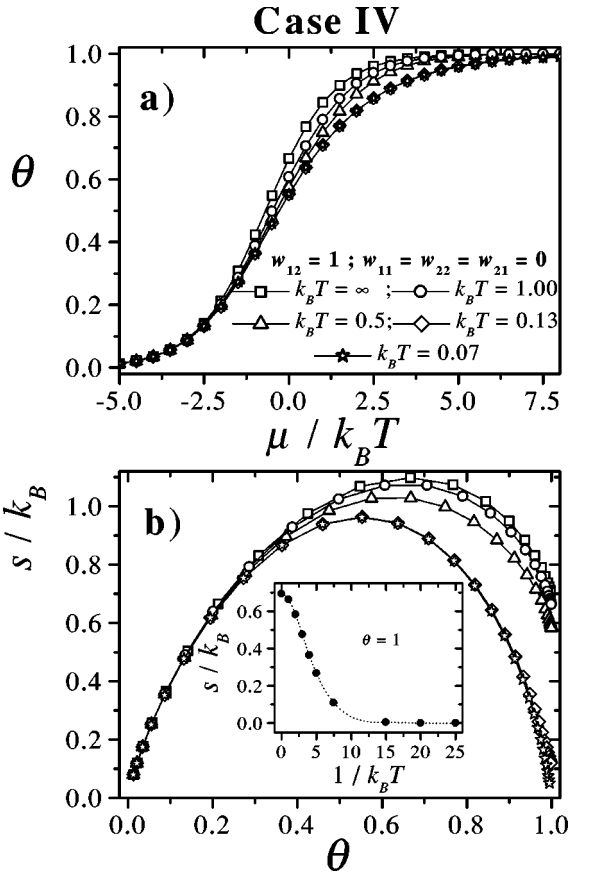

FIG. 6. As Fig. 5 for case IV.

In the thermodynamical limit, Eq. (26) is reduced to

$$B^2 - B - 1 = 0, \tag{27}$$

where we have supposed $B > 1$. The solutions of Eq. (27) are $B_1 = (1+\sqrt{5})/2$ and $B_2 = (1-\sqrt{5})/2$. We choose B_1, due to $B_2 < 1$. Finally, from Eq. (24),

$$\frac{s(\theta=1,T=0)}{k_B} = \ln B_1 = \ln\left(\frac{1+\sqrt{5}}{2}\right) = 0.4812. \tag{28}$$

Figures 6–9 show a study as in Fig. 5 for cases IV–VII, respectively. A qualitative difference appears in Figs. 6–9 with respect to Fig. 5, namely, $s(\theta=1,T=0)/k_B = 0$ for cases IV–VII, while $s(\theta=1,T=0)/k_B \neq 0$ for case III. The explanation for this behavior is as follows.

Case IV. Due to $w_{12} > 0$, the adsorbate avoids the formation of 1-2 pairs. As a consequence, two states are possible at full coverage in the ground state. In the first, the adatoms belong to the 1-specie and the structure of the adsorbate is (111111 . . .). In the second, the adsorbate is formed for 2-particles and the structure of the adsorbate is (222222 . . .). Under these considerations, the configurational entropy per site in the thermodynamical limit, $s(\theta=1,T=0)/k_B$, results in

$$\frac{s(\theta=1,T=0)}{k_B} = \lim_{M\to\infty} \frac{\ln 2}{M} = 0. \tag{29}$$

Case V. In this case, the adsorbate avoids the formation of 11 and 22 pairs. In the ground state, a structure of alternating 1 and 2 (12121212 . . . .) is formed at full coverage. The degeneration of this structure is two and the configurational entropy per site in the thermodynamical limit is zero.

Cases VI and VII. In both cases, the ground state is nondegenerate and the structure of the adsorbate at full coverage is (222222 . . .). Consequently, the configurational entropy per site in the thermodynamical limit is zero.

As it was discussed above, in five cases (II–VII), the configurational entropy per site at full coverage tends to zero as the temperature is diminished. For these cases, the temperature dependence of $s(\theta=1,T)/k_B$ is shown in Fig. 10. The approach to the asymptotic value, $s(\theta=1,T=0)/k_B = 0$, is related to the set of lateral interactions between the adparticles. Thus, the case VII requires values of $k_BT \approx 0.2$, in order to reach the ground state. On the other hand, intermediate [low] values of k_BT (≈ 0.1) [≈ 0.05] are required for cases II and IV [V and VI].

From the analysis of the cases I–VII, two well-differentiate behaviors can be found for the adsorption properties.

(i) For cases I and II, the ground state is characterized by the existence of two adsorption regimes, separated by the

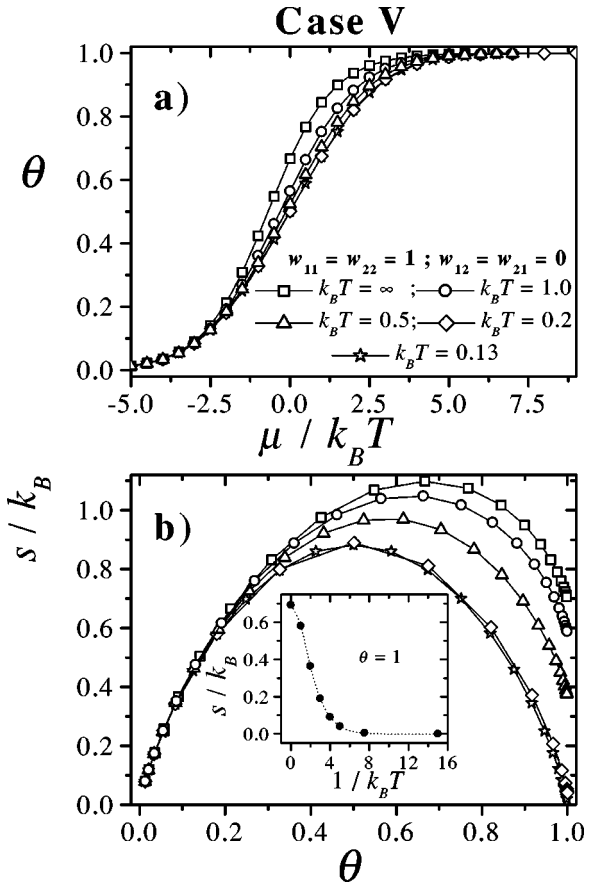

FIG. 7. As Fig. 5 for case V.

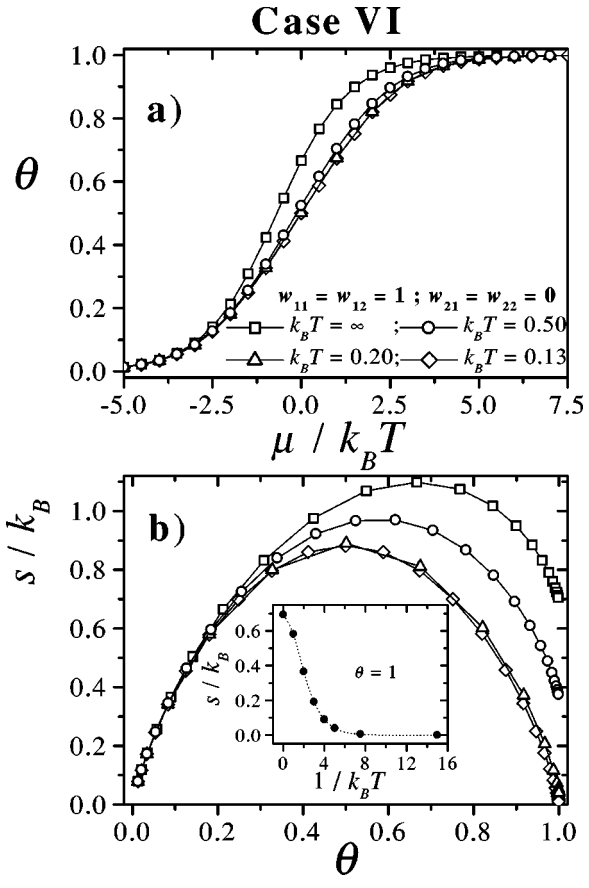

FIG. 8. As Fig. 5 for case VI.

formation of a structure in the adsorbate at intermediate coverage. This structure is reflected as a plateau in the adsorption isotherm or as a minimum in the configurational entropy per site.

(ii) For cases III–VII, only one adsorption regime appears and the adsorption properties vary smoothly in the entire range of coverage.

A third behavior can be expected by mixing the cases I and II. For this purpose, we started from the case I and then we diminished the value of w_{21} till the case II was recovered ($w_{21}=0$). In contrast to Figs. 2–10, now we fixed the temperature and varied the lateral interactions. The results of this study are shown in Figs. 11 and 12. The curves were obtained for $k_BT=1$, $w_{11}=w_{12}=w_{22}=12.5$, and different values of w_{21} ($=12.5,10,7.5,5,2.5,0$).

In Fig. 11 we present the adsorption isotherm (a) and the configurational entropy per site (b). It can be seen that all curves are contained between the two limit cases: the one corresponding to case I and the other corresponding to case II. The more interesting behaviors appear for intermediate values of w_{21} (≈ 5), where three adsorption regimes can be clearly distinguished from the plateaus (minima) in the adsorption isotherm (entropy): (i) for $0<\theta<1/2$, the sites are filled avoiding nearest-neighbor (NN) occupancy; (ii) for $1/2<\theta<\theta_m$, the particles absorb until a sequence (210210210 . . .) is formed on the lattice; and (iii) for $\theta_m<\theta<1$, the filling is completed.

A more detailed study, about the adsorption regimes presented in Fig. 11, can be performed through analyzing the differential heat of adsorption versus coverage, $q_d(\theta)$. In this sense, in Fig. 12(a) we present the curves of $q_d(\theta)$ corresponding to the cases of Fig. 11. As it can be noted, the differential heat of adsorption appears as a very sensitive quantity to the adsorption process. The behavior of q_d could be analyzed by focusing our attention on two main features: plateaus and steps. The plateaus indicate the existence of different adsorption regimes and the steps correspond to the critical coverage and separate different adsorption regimes. Based on these elements, in Fig. 12(b) we present $q_d(\theta)$ for a typical intermediate case (obtained by mixing the cases I and II). The plateaus clearly denote the three adsorption regimes. In the first regime ($0\leqslant\theta<1/2$), the adatoms do not interact with each other, and the adsorption desorption of a monomer involves a $q_d=0$; for $1/2\leqslant\theta<\theta_m$, the energy cost upon adsorption of a particle can be estimated by considering the adsorption of an incoming atom on the structure at $\theta=1/2$. The process is shown in Fig. 13. As it can be seen, the adsorption of one particle creates two pairs 21 on the lattice. Accordingly, the value of q_d in this regime is $q_d=-2w_{21}$ (in the particular case of the figure, $q_d=-10$). In the ground state, the final configuration at θ_m is a repetition of the sequence (210). Finally, for $\theta_m\leqslant\theta<1$, the process can be easily understood by analyzing the simultaneous adsorption of two particles, as it is shown in Fig. 14. The initial state corresponds to a structure as in Fig. 14(a). In the final state, two particles were adsorbed and a pair 12 was changed in

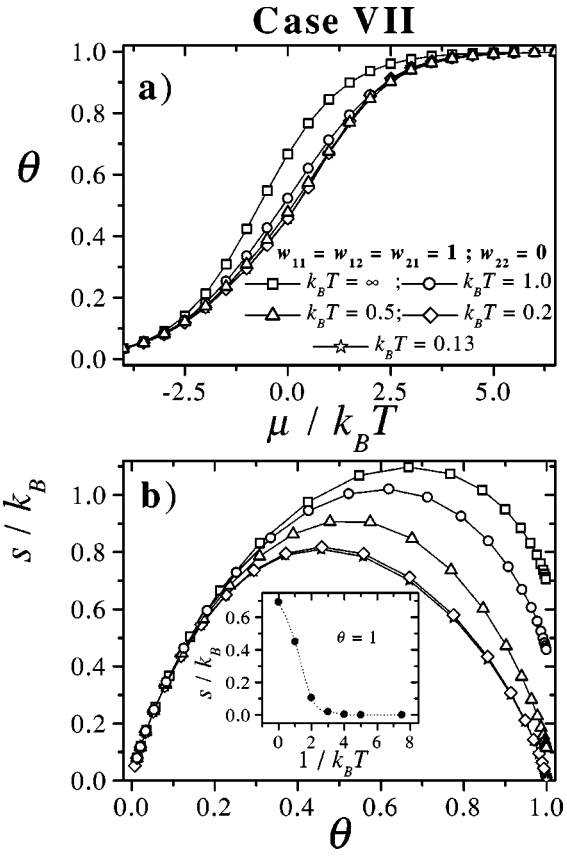

FIG. 9. As Fig. 5 for case VII.

order to form a pair 21. This process involves an energy variation of $3w_{12}+w_{21}$. As the differential heat of adsorption measures the variation of energy per particle, the value of q_d in this regime is $q_d=-(3w_{12}+w_{21})/2$ (in the particular case of the figure, $q_d=-21.5$).

The type of isotherm presented in Fig. 11(a) has been reported recently for CH_4 adsorbed in $AlPO_4-5$ [17]. As an example, experimental isotherms of $CH_4/AlPO_4-5$ at $T=77.35$ K and $T=96.5$ K from Martin *et al.* [17] are shown in Fig. 15 (empty symbols). The double-stepped isotherms

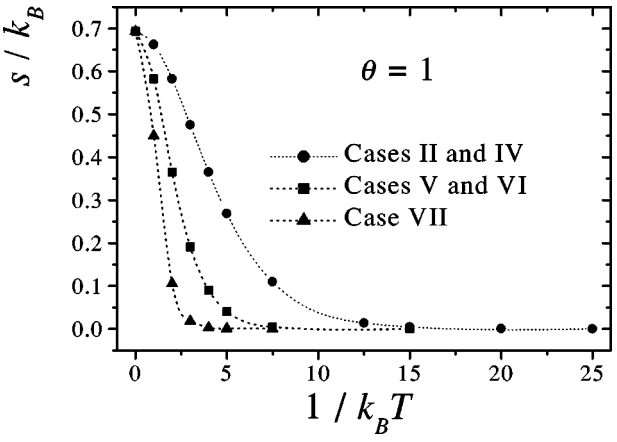

FIG. 10. Temperature dependence of the configurational entropy per site at full coverage, $s(\theta=1,T)/k_B$, for the different cases indicated in the figure.

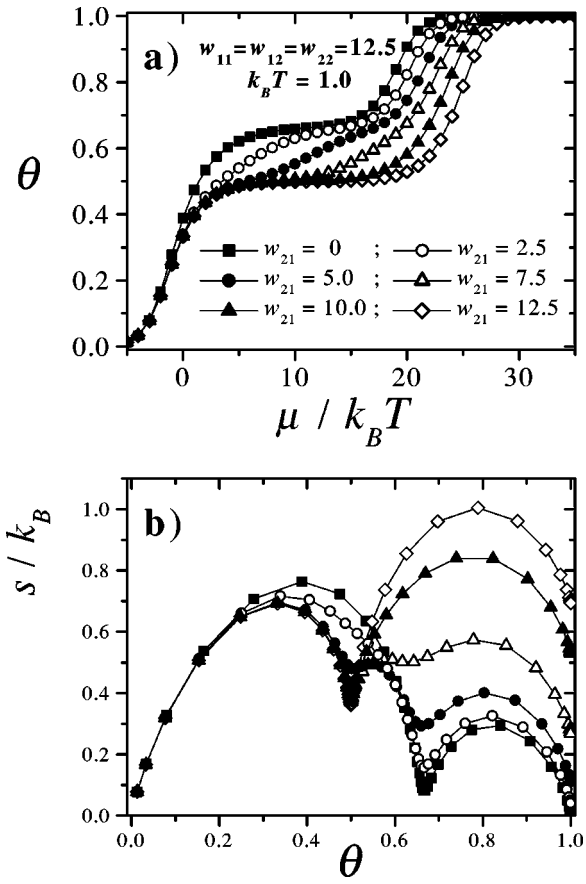

FIG. 11. Adsorption isotherm (a) and configurational entropy per site vs coverage (b) for monomers adsorbed with $k_BT=1$, $w_{11}=w_{12}=w_{22}=12.5$, and different values of w_{21}.

could be the consequence of a rearrangement of molecules within the tubules in such a way that, although ad-ad interaction energy increases (in absolute values) upon rearrangement, gas-solid interaction energy decreases, giving a net repulsive effect in the adsorption isotherm as well as in the isosteric heat of adsorption. Lachet *et al.* [14] propose that the isosteric heat of adsorption increases from zero coverage up to $\theta=2/3$. This increase is mainly due to attractive interactions between neighboring methane. The attraction between the admolecules for $\theta<2/3$ favors very much the adsorption of pairs of methane molecules as small clusters which look like a CH_4 dimers chain. For $\theta>2/3$, even though the ad-ad interactions increase, the gas-solid interaction energy decreases owing to the stronger repulsion in the new equilibrium positions.

By following the arguments given in the detailed study of Figs. 11 and 12, we propose the case of attractive w_{21} interactions and repulsive values of w_{11}, w_{12}, and w_{22} as a model to interpret the results of Ref. [17]. This analysis is shown in Fig. 15, where solid symbols correspond to theoretical adsorption isotherms at the same temperatures as the ones in the experimental results. The energetic parameters (shown in figure) were adjusted to fit the experimental curves. [We should keep in mind that the mismatch between the equilibrium separation of the intermolecular interaction and the lattice constant along the nanochannels plays a fundamental

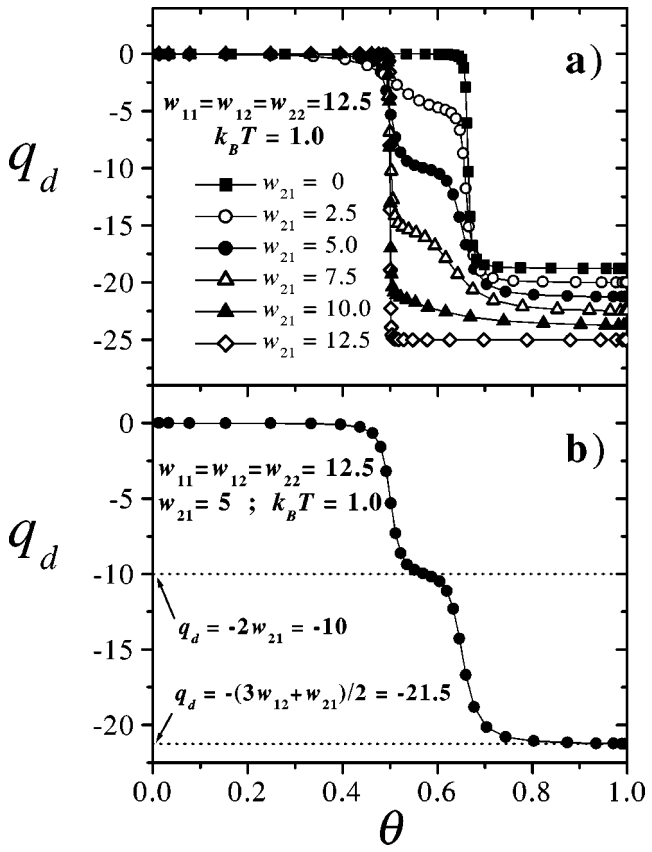

FIG. 12. (a) Differential heat of adsorption vs coverage for the same cases plotted in Fig. 11(b). Differential heat of adsorption vs coverage for $k_BT=1$ and the lateral interactions indicated in the figure.

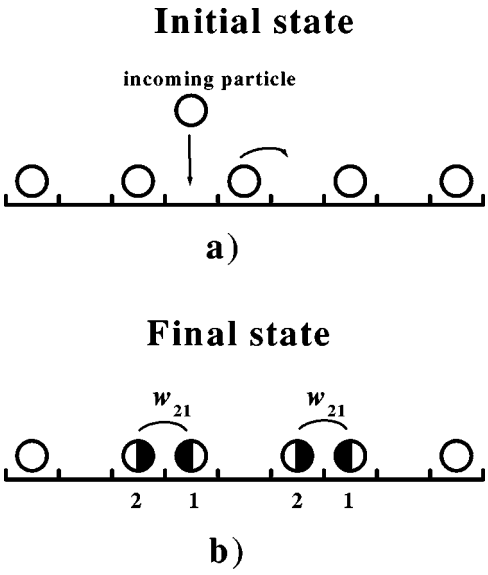

FIG. 13. Snapshots of the adsorbate at $1/2<\theta<\theta_m$ showing the elementary step necessary to adsorb a particle: (a) initial state; (b) final state where an adsorbed atom has been shifted to the right (forming a pair 21) and a new particle has been adsorbed (forming a pair 21).

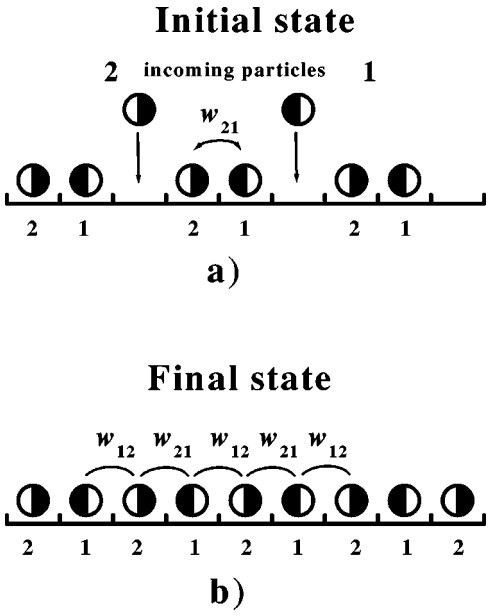

FIG. 14. Snapshots of the adsorbate at $\theta_m<\theta<1$ showing the elementary step necessary to adsorb two particles: (a) initial state; (b) final state where a pair 12 has been inverted (forming a pair 21), a 1-particle has been adsorbed (forming a pair 21 and a pair 12) and a 2-particle has been adsorbed (forming a pair 21 and a pair 12).

role in the adsorption process and it is responsible for the asymmetry observed in the experimental isotherms. This effect, which characterizes the real systems, does not appear in our simplified model due to the fact that the adsorbate is assumed in registry with the lattice constant. Then, although CH_4 is one of the most symmetric molecules, the fitted asymmetric lateral interactions represent an effective way of including the full effect of (i) adsorbate-adsorbate interactions; (ii) adsorbate-adsorbent interactions; and (iii) adsorbate/surface geometry.] The experimental isotherms are much steeper at low and high coverages than the ones for the

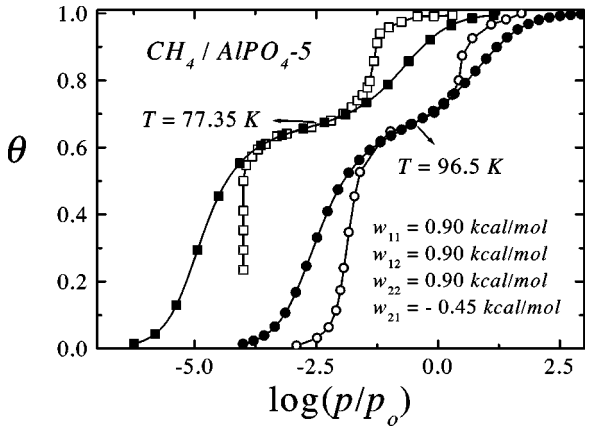

FIG. 15. Comparison between experimental isotherm of $CH_4/AlPO_4-5$ from Ref. [17] (open squares, $T=77.35$ K; open circles, $T=96.5$ K) and theoretical isotherm from Eq. (11) (solid squares, $T=77.35$ K, $w_{11}=w_{12}=w_{22}=$kcal/mol, and $w_{21}=$kcal/mol, solid circles, $T=96.5$ K, $w_{11}=w_{12}=w_{22}=$kcal/mol, and $w_{21}=$kcal/mol). p_o is a reference pressure.

theoretical model. However, a fair agreement for the slope and broadness of the plateau is observed.

Finally, it is worth noticing that although the model considered here is highly idealized, the main reason of the comparison in Fig. 15 is to highlight that the physical nature of the plateau both in experiments and the model could be the same.

IV. CONCLUSIONS

The exact forms of the thermodynamic functions for interacting nonsymmetrical adsorbates in a one-dimensional space were presented. The study was restricted to the case of repulsive lateral interactions among adsorbed particles (with the exception of Fig. 15, where attractive w_{21} interactions were included in the fitting of experimental data). If pure attractive lateral interactions were considered, a sharp jump, which is very similar to a condensation transition, would be observed in the isotherms at low temperatures. However, it is well known that no phase transition develops in a one-dimensional lattice gas of interacting particles [7].

A rich variety of behaviors has been obtained for different values of the lateral interactions. In the particular case of $w_{11}=w_{12}=w_{21}=w_{22}$, the results of TMM were compared with the closed exact solution corresponding to the well-known problem of the one-dimensional interacting lattice gas. The comparison allowed us to corroborate the accuracy and validity of the calculations obtained by using TMM.

With respect to the temperature dependence of the adsorption isotherm and the configurational entropy per site versus coverage, the more interesting behaviors were found at low temperatures. In the limit of $T=0$ (ground state), different structures were observed in the adsorbate. The effect of these structures on the adsorption process was widely discussed.

Experimental results for methane adsorbed in $AlPO_4-5$ were used to test the applicability of the exact isotherm, Eq. (11). This analysis demonstrated that the theoretical calculations may have interesting potential application in adsorption equilibrium for adsorbates in quasi-one-dimensional materials (carbon nanotubes, $AlPO_4-5$, $SAPO-5$, etc.).

The present study shows that the adsorption thermodynamics of nonsymmetrical particles has many different features compared to the standard lattice gas of monomers. This encourages the study of the critical behavior and the thermodynamic functions for attractive and repulsive nonsymmetrical adatoms in 2D. In this sense, future efforts will be directed to (a) include attractive lateral interactions between the adparticles, (b) perform new analytical expressions for the thermodynamic functions in higher dimensions, and (c) compare the theoretical results with Monte Carlo simulations.

ACKNOWLEDGMENTS

The authors are thankful to Professor G. Zgrablich for the critical reading of the manuscript. This work was partially supported by the CONICET (Argentina) and Fundación Antorchas (Argentina).

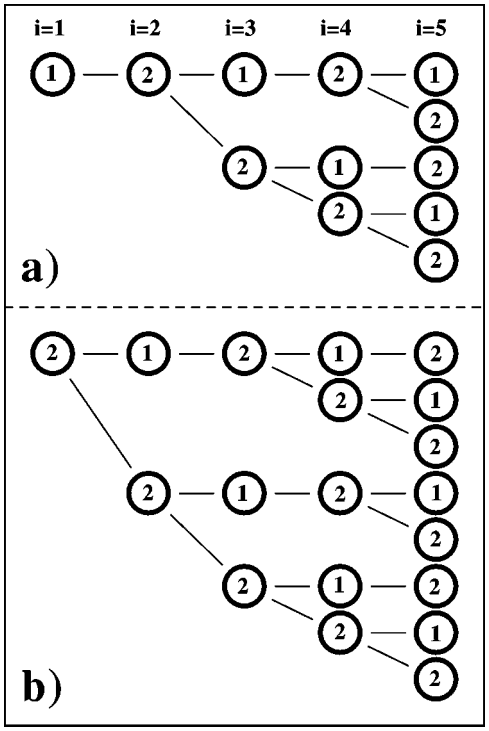

FIG. 16. Diagrams showing the number of different configurations of the ground state, g_M, for $M=5$, $w_{11}=w>0$, $w_{12}=w_{21}=w_{22}=0$ (case III), and $\theta=1$ (full coverage). Part (a) [(b)] presents the configurations with a 1[2]-particle adsorbed on the site $i=1$ ($c_1=1$ [2]).

APPENDIX

Let us discuss a procedure for calculating the number of different configurations (degeneracy) of the adsorbate at $T=0$ and $\theta=1$, g_M, for case III. As an example, the available configurations for a lattice of size $M=5$, with open boundary conditions, are shown in Fig. 16. Due to $w_{11}>0$, the adsorbate avoids the formation of 11 pairs. In part (a) [(b)] we present the configurations with a 1[2]-particle adsorbed on the site $i=1$ ($c_1=1$ [2]). For each sequence, the lattice site $i=5$ can be occupied by a 1- or 2-particle. Then,

$$g_M=g_{M,1}+g_{M,2}, \tag{A1}$$

where $g_{M,1}$ and $g_{M,2}$ represent the total number of configurations with $c_M=1$ and $c_M=2$, respectively. In this case, $g_5=13$, $g_{5,1}=5$, and $g_{5,2}=8$.

In addition, each configuration for a lattice of size $M=4$ with $c_4=1$ generates one configuration for a lattice with $M=5$ (with $c_5=2$). On the other hand, each configuration for a lattice of size $M=4$ with $c_4=2$ generates two configurations for a lattice with $M=5$ (with $c_5=1$ or 2). By generalizing this argument, it is possible to write

$$g_{M,1}=g_{M-1,2} \tag{A2}$$

and

$$g_{M,2}=g_{M-1,1}+g_{M-1,2}=g_{M-1}. \tag{A3}$$

Equations (A.1)–(A.3) lead to

$$g_M = g_{M,1} + g_{M,2} = g_{M-1,2} + g_{M-1}. \quad \text{(A4)}$$

By using Eq. (A.3) in terms of $M-1$ and $M-2$, we can write

$$g_{M-1,2} = g_{M-2}. \quad \text{(A5)}$$

Finally, from Eqs. (A4) and (A5), we obtain

$$g_M = g_{M-2} + g_{M-1}. \quad \text{(A6)}$$

[1] W.A. Steele, *The Interaction of Gases with Solid Surfaces* (Pergamon Press, New York, 1974).

[2] J.G. Dash, *Films on Solid Surfaces* (Academic Press, New York, 1975).

[3] L.W. Bruch, M.W. Cole, and E. Zaremba, *Physical Adsorption: Forces amd Phenomena* (Oxford Science Publications, Oxford, 1997).

[4] W. Rudziński and D.H. Everett, *Adsorption of Gases on Heterogeneous Surfaces* (Academic Press, New York, 1992).

[5] M.J. Jaroniec and R. Madey, *Physical Adsorption on Heterogeneous Surfaces* (Elsevier, Amsterdam, 1988).

[6] W. Rudziński, W.A. Steele, and G. Zgrablich, *Equilibria and Dynamics of Gas Adsorption on Heterogeneous Solid Surfaces* (Elsevier, Amsterdan, 1996).

[7] T.L. Hill, *An Introduction to Statistical Thermodynamics* (Addison-Wesley, Reading, MA, 1960).

[8] V.P. Zhdanov, *Elementary Physicochemical Processes on Solid Surfaces* (Plenum Press, New York, 1991).

[9] Y.K. Tovbin, *Theory of Physical Chemistry Processes at a Gas-Solid Interface* (Mir, Moscow, 1991).

[10] A.J. Ramirez-Pastor, F.M. Bulnes, and J.L. Riccardo, Surf. Sci. **426**, 48 (1999).

[11] A.W. Adamson, *Physical Chemistry of Surfaces* (Wiley, New York, 1990).

[12] S.J. Gregg and K.S.W. Sing, *Adsorption, Surface Area, and Porosity* (Academic Press, New York, 1991).

[13] A. Boutin, R.J.-M. Pellenq, and D. Nicholson, Chem. Phys. Lett. **219**, 484 (1994).

[14] V. Lachet, A. Boutin, R.J.-M. Pellenq, D. Nicholson, and A.H. Fuchs, J. Phys. Chem. **100**, 9006 (1996).

[15] R. Radhakrishnan and K. Gubbins, Phys. Rev. Lett. **79**, 2847 (1997).

[16] T. Maris, T.J.H. Vlugt, and B. Smit, J. Phys. Chem. **102**, 7183 (1998).

[17] C. Martin, N. Tosi-Pellenq, J. Patarin, and J.P. Coulomb, Langmuir **14**, 1774 (1998).

[18] J.P. Coulomb, C. Martin, N. Floquet, Y. Grillet, and J. Patarin, in *Proceedings of the Sixth International Conference on Fundamentals of Adsorption*, edited by F. Meunier (Elsevier, Amsterdam, 1998), p. 165.

[19] W.H. Weinberg, Annu. Rev. Phys. Chem. **34**, 217 (1983).

[20] A.J. Phares and F.J. Wunderlich, J. Math. Phys. **27**, 1099 (1986).

[21] A.J. Phares, F.J. Wunderlich, J.D. Curley, and D.W. Grumbine, Jr., J. Phys. A **26**, 6847 (1993).

[22] A.J. Ramirez-Pastor, T.P. Eggarter, V. Pereyra, and J.L. Riccardo, Phys. Rev. B **59**, 11027 (1999).

[23] A.J. Ramirez-Pastor, A. Aligia, F. Romá, and J.L. Riccardo, Langmuir **16**, 5100 (2000).

[24] F. Romá, A.J. Ramirez-Pastor, and J.L. Riccardo, J. Chem. Phys. **114**, 10932 (2001).

[25] J.L. Hock and R.B. McQuistan, J. Chem. Phys. **89**, 2292 (1988).

[26] A.V. Myshlyavtsev and V.P. Zhdanov, Chem. Phys. Lett. **162**, 43 (1989).

[27] A.V. Myshlyavtsev and V.P. Zhdanov, J. Chem. Phys. **92**, 3909 (1990).

[28] A.V. Myshlyavtsev and V.P. Zhdanov, Surf. Sci. **291**, 145 (1993).

[29] A.V. Myshlyavtsev, A.A. Stepanov, C. Uebing, and V.P. Zhdanov, Phys. Rev. B **52**, 5977 (1995).

[30] A. Aligia, Phys. Rev. B **47**, 15308 (1993).

[31] R. Kikuchi, Phys. Rev. **81**, 988 (1951).